Scanning tunneling spectroscopy on Co(0001): Spectroscopic signature of stacking faults and dislocation lines

J. Wiebe,[1,*] L. Sacharow,[1] A. Wachowiak,[1,†] G. Bihlmayer,[2] S. Heinze,[1] S. Blügel,[2] M. Morgenstern,[1] and R. Wiesendanger[1]
[1]*Institute of Applied Physics and Microstructure Research Center, University of Hamburg, Jungiusstraße 11, 20355 Hamburg, Germany*[‡]
[2]*Institut für Festkörperforschung, Forschungszentrum Jülich, 52425 Jülich, Germany*
(Received 1 December 2003; revised manuscript received 26 February 2004; published 8 July 2004)

The growth morphology and electronic structure of Co(0001) grown on W(110) are studied using scanning tunneling microscopy and scanning tunneling spectroscopy (STS) at $T=6$ K. Depending on growth conditions, continuous Co films or Co islands on top of a wetting layer are formed. Within the continuous films, dislocation lines appear and increase in density after annealing. Co islands and films exhibit dI/dV curves with a pronounced peak at −0.3 eV below the Fermi energy. The intensity of this peak is changing in different areas of the surface. Using monolayer high islands with a different shape deposited on the same Co layer we attribute the different intensity to a different stacking of the Co surface. The change in intensity is reproduced by first-principles electronic structure calculations, which reveal that the peak is caused by a $d_{3z^2-r^2}$-like surface resonance of a minority-spin character more strongly coupled to the bulk states in the case of hcp (*ABA*) stacking than in the case of fcc (*ABC*) stacking. An increased STS intensity of the surface resonance was also found above dislocation lines located at the Co/W interface.

DOI: 10.1103/PhysRevB.70.035404 PACS number(s): 73.20.At, 68.55.−a, 68.37.Ef

I. INTRODUCTION

Nowadays there is an increasing interest in layered magnetic thin-film structures because they exhibit effects such as the giant magneto resistance or the tunneling magneto resistance usable in data storage devices.[1] Co is often used as a ferromagnetic material in such structures, in particular for model systems.[2–6] It is well known that the performance of the model system depends crucially on the electronic states at the Co interface. Thus, the knowledge about interface defects such as stacking faults is important.

Indeed, it has been shown recently by Vázques de Parga *et al.*[7] using scanning tunneling spectroscopy (STS) on Co/Cu(111) that the electronic structure of the Co(0001) surface depends sensitively on stacking. Nevertheless the spectroscopic results are contradictory to other STS measurements by Pietzsch *et al.*,[8] Diekhöner *et al.*,[9] and Okuno *et al.*[10] One possible explanation for the discrepancy is an intermixing of Co and Cu that depends sensitively on the preparation process.[11,12] A way to circumvent this effect is the use of a W(110) substrate which excludes any intermixing. Nevertheless, the electronic properties of Co/W(110) have only been investigated by spatially averaging techniques where stacking fault effects are not detectable.[13–19]

Apart from the question of the influence of stacking, there are also contradictory results concerning the surface-related states of Co(0001) itself. Early angle resolved photoelectron spectroscopy (ARUPS) measurements claimed an *sp*-like surface state at −0.3 eV with respect to the Fermi energy,[20,21] which was later ascribed to a $d_{3z^2-r^2}$-like state.[13] Some of the recent STS experiments confirm the existence of this state by showing a peak at −0.31 eV or at a slightly different energy −0.43 eV.[8–10] In contrast, Vázques de Parga *et al.*[7] found no spectroscopic features below E_F.

Using first-principle calculations, Diekhöner *et al.*[9] assigned the STS peak below the Fermi energy to a $d_{3z^2-r^2}$-like state of a minority-spin character. This is in accordance with the interpretation of the photoemission results. A similar conclusion is drawn from the analysis of the STS results by Okuno *et al.*[10] However, both papers imply that the peak in STS originates from a $d_{3z^2-r^2}$-like surface state at the $\bar{\Gamma}$ point, while photoemission calculations by Braun *et al.*[22] imply that the photoemission peak originates from *d* states away from $\bar{\Gamma}$.

Here we present the first STS study of Co on W(110). We found different Co morphologies as continuous films or islands depending on preparation conditions, but on each system we observed distinct regions which we identified as stacking faults. Moreover, we found a peak in STS at −0.3 eV, similar to the one which was measured on the Co/Cu(111) system.[8–10] This peak turned out to be sensitive to the stacking at the continuous film or island surface as well as to dislocation lines within the continuous films. In order to identify the origin of the peak we performed first-principles electronic structure calculations. They help to assign the peak to a surface *resonance* with a minority-spin character being mainly $d_{3z^2-r^2}$-like. But, in contrast to previous results,[9,10] the corresponding states are located in a ring-like region *off* from the $\bar{\Gamma}$ point at a distance of approximately 0.4 Å^{-1}, and not at $\bar{\Gamma}$. Importantly, it turned out that the surface resonance is coupled more weakly to bulk *d* states for fcc stacking than for hcp stacking. This leads to a higher localization of the surface resonance in the surface layer for fcc stacking and, respectively, to a 20% larger vacuum density of states being detectable by STS. In turn, the $d_{3z^2-r^2}$-like surface resonance at −0.3 eV can be used to spectroscopically identify the local stacking of Co(0001).

II. EXPERIMENTAL DETAILS

All experiments were performed in two different UHV systems described elsewhere.[23–25] One was used for room

temperature (RT) scanning tunneling microscopy (STM) and STS,[24,25] the other for STM/STS at $T=6$ K.[23] The base pressure of both systems is in the 10^{-11} mbar range. We used either *ex situ* mechanically sharpened PtIr or electrochemically etched W tips, both prepared afterwards by field emission in UHV. Two different W(110) single crystals with an average terrace width of $\approx$10 nm and $\approx$200 nm, respectively, were used as substrates. They were cleaned by repeated cycles of heating at $T=1500$ K in an oxygen atmosphere of 5×10^{-7} mbar and subsequent flashing to 2500 K.[26] After this preparation, both crystals gave a sharp (1×1) low-energy electron diffraction (LEED) pattern. Several monolayer (ML) thick Co films were deposited at RT with an *e*-beam evaporator at a rate of 0.1-0.2 ML/min. During deposition the pressure remained below 2×10^{-10} mbar. The rate was calibrated by STM images of films with a thickness below 0.5 ML that are known to grow pseudomorphically on the W substrate.[13,15,27–30] This results in a relative accuracy better than 20%. In the following, the notation of 1 ML corresponds to the equivalent of one pseudomorphic layer of Co on W(110). Films thicker than 1 ML were subsequently thermally annealed for 10 min at temperatures ranging from 400–600 K. The temperature was preliminarily calibrated with a thermocouple attached to the tungsten sample holder to which the W(110) crystal is mounted via tungsten wires. This leads to an accuracy of ±15 K for heating in the RT-STM system.

STM images were recorded in the constant-current mode at a stabilizing current I_{stab} with the bias voltage V_{stab} applied to the sample ("constant-current image"). The vertical and lateral sensitivity of the tube scanner was calibrated on monoatomic steps of the W(110) substrate and on the unit cell of the InAs(110) surface,[31] respectively, leading to an accuracy of better than 5%. Most images are raw data, except that a plane has been substracted to compensate for misalignment of tip and sample. We enhanced the contrast of some STM images by mixing the constant-current image with its derivative along the fast scan direction.

To obtain spectroscopic information a small ac modulation voltage V_{mod} ($\nu\approx1.5$ kHz) is added to V_{stab}. At every point (x,y) of the image, the tip is stabilized at V_{stab} and I_{stab}, the feedback is opened, and a $dI/dV(V,x,y)$ curve is measured by the lock-in technique. The resulting $dI/dV(V,x,y)$ signal is a measure of the local density of states (LDOS) of the sample surface below the tip apex with V corresponding to the electron energy with respect to the Fermi level E_F.[32–34] Additionally, the $dI/dV(V)$ signal is recorded during constant-current images with closed feedback giving a so-called dI/dV map at an energy corresponding to V_{stab}.

III. EXPERIMENTAL RESULTS

A. Structural properties

1. Previous results

The growth of Co on W(110) has been investigated extensively[13,15,27–29] although only few studies have been reported using STM.[17,30,35] Results of importance for this publication will be succinctly reviewed in the following. Co

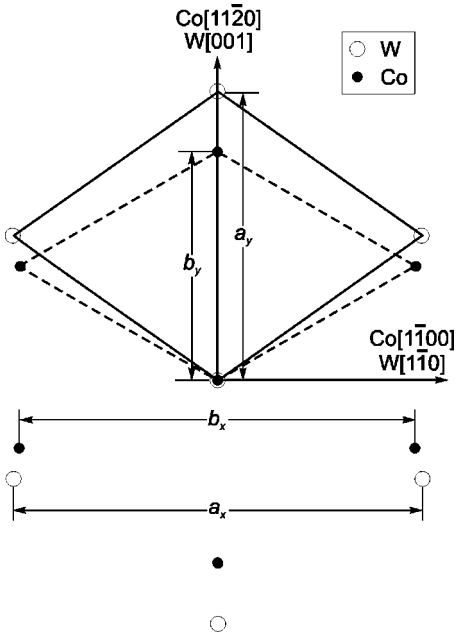

FIG. 1. Diagram showing the unit cells of the W and the Co surface oriented according to the Nishiyama-Wassermann orientation. a_i and b_i denote the diagonal lengths of the unit cells of W (solid lines) and Co (dashed lines), respectively, were $i=x$ points in the $[1\bar{1}0]$ direction and $i=y$ points in the [001] direction of the W(110) substrate.

grows in the Nishiyama-Wassermann orientation, which means that the Co(0001) plane is parallel to the W(110) plane and Co $[11\bar{2}0]\|$W[001]. A comparison of the unit cells of bulk W and bulk Co aligned accordingly is shown in Fig. 1. The diagonal lengths of the unit cells are given by $a_y^{bulk}=3.165$ Å and $a_x^{bulk}=\sqrt{2}a_y^{bulk}=4.476$ Å for *W* and by $b_y^{bulk}=2.507$ Å and $b_x^{bulk}=\sqrt{3}b_y^{bulk}=4.342$ Å for Co, where x denotes the $[1\bar{1}0]$ direction and y the [001] direction of the W(110) substrate.[29] In the Co/W(110) film, the strain is given by

$$\varepsilon_i=\frac{(b_i-b_i^{bulk})}{b_i^{bulk}},\ i=x,y, \tag{1}$$

where b_i now denotes the mean strained value. Up to approximately 0.5 ML the growth is pseudomorphic,[30] which means $\varepsilon_x=3.1\%$ and $\varepsilon_y=26.2\%$. For increasing coverage a transition to a (8×1) LEED pattern has been observed. It is generated by areas of a closed-packed monolayer with perfect registry in the x direction ($\varepsilon_x=3.1\%$) and a commensurable structure in the y direction, where every fifth adsorbate row coincides with every fourth substrate row ($\varepsilon_y=+1\%$). These areas coexist with areas of the pseudomorphic monolayer.[30] The (8×1) pattern was observed for coverages up to approximately 2 MLs. Above this coverage, the structure is slightly changed in the y direction towards a (7.1×1) structure leading to $\varepsilon_y=-1.45\%$. This structure persists up to 10 ML, where the strain in the x and y directions as well as in the direction of the surface normal, is found to be reduced exponentially. The latter is probably caused by the

appearance of misfit dislocations at the interface.[13]

The described results for films thicker than 1 ML were obtained for annealing temperatures below $T=500$ K, where two-dimensional growth is predominant. For annealing temperatures above 500 K the film breaks up into three-dimensional islands[17,27,35,36] sitting on a closed Co wetting layer.[36] The three-dimensional island growth probably leads to smaller strain due to a possible relaxation within each island.

All reported LEED results do not explicitly distinguish between hcp (*ABA*) and a possible fcc (*ABC*) stacking in the Co films. Though bulk Co is hcp at RT and fcc only above $T\approx 700$ K,[37] thin Co films often show fcc stacking even at RT.[38,39] Knoppe *et al.*[13] compare photoelectron diffraction data with calculations for hcp and fcc stacking. This has been done for a 7 ML and a 12 ML Co film annealed to 450 K, i.e., in the continuous film growth morphology. The agreement between measurement and calculation favors hcp stacking but the authors cannot exclude that some areas of the surface are still fcc stacked.[40] To our knowledge, there are no corresponding statements about stacking for the island morphology.

2. Growth modes

Figures 2(a)–2(c) show constant-current images of a 3 ML Co film grown on the W crystal with 10 nm terrace width. The film was annealed at increasing temperature as indicated in the images. In agreement with previous results we find two-dimensional growth below ≈500 K with a typical corrugation of ±1 ML as visible in the line profile *A* of Fig. 2(d). Three-dimensional island growth is found for higher annealing temperatures as shown in Figs. 2(b) and 2(c). As obvious from the line profile *B* in Fig. 2(d) the islands are wedge shaped due to the step edges of the underlying substrate and extended preferentially parallel to the W step edges as reported previously.[17,35] The island surface is atomically flat apart from a height modulation of 0.1 Å. It is barely visible in Fig. 2(c) as faint stripes, which are oriented along the W step edges. As for Gd and Fe islands on W(110) the height modulation is induced by the smaller step size of Co(0001) (2.04 Å) compared to W(110) (2.24 Å).[41,42] For increasing temperature there are less islands which are partly higher and more extended along the step edges. After annealing to 500 K [Fig. 2(b)], the largest islands have a lateral extension of 40×60 nm^2 and a height of about 5.5 ML, while at 570 K [Fig. 2(c)] their lateral size is 50×200 nm^2 and the height is about 6.5 ML.

Figures 2(e)–2(g) show constant-current images of a 10 ML Co film grown on the W crystal with a 200 nm terrace width. The film was annealed at different temperatures below the critical temperature for island growth as indicated. Again, layer by layer growth is found in this temperature range. Obviously the roughness is reduced for increasing annealing temperature. While five open layers, i.e., layer 6 to layer 10, are distinguishable on the film annealed at 350 K as can be seen in the line profile *C* of Fig. 2(h), only three open layers are found in the film annealed at 400 K. Moreover, the lateral extension of the remaining islands is much larger upon higher annealing. Finally, the film annealed at 450 K

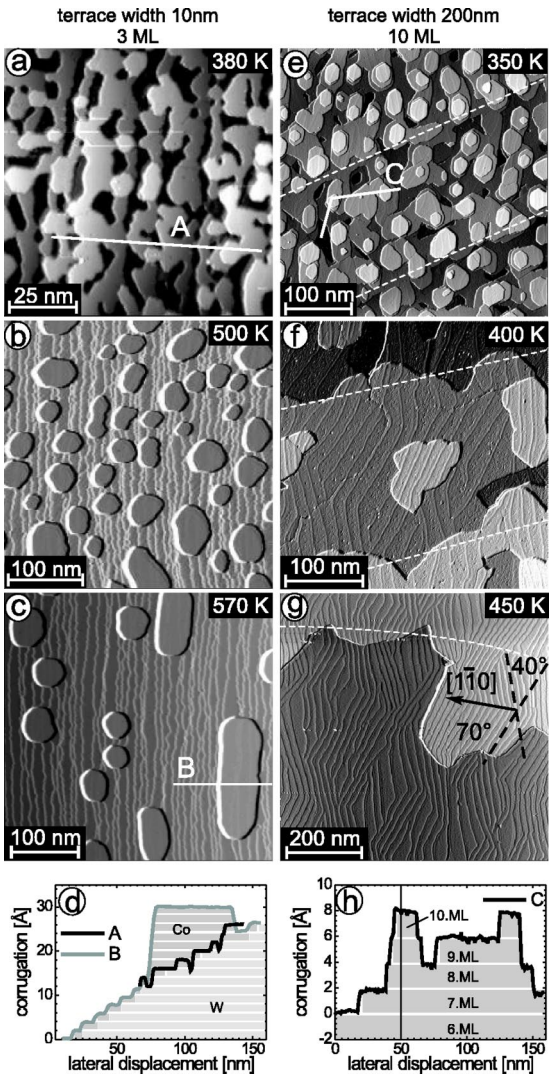

FIG. 2. Growth of Co on W(110) at different annealing temperatures as indicated in the images. (a)–(c) Constant-current images of 3 ML Co on a W(110) crystal with an average terrace width of 10 nm [(a) and (b) $I=0.3$ nA, $V=-0.3$ V; (c) $I=0.2$ nA, $V=-0.8$ V; $T=300$ K)]. (d) Line profiles along the lines *A* and *B* in (a) and (c), respectively. (e)–(g) Constant-current images of 10 ML Co on a W(110) crystal with an average terrace width of 200 nm. The step edges of the W substrate run along the white dashed lines [(e) $I=0.6$ nA, $V=-0.33$ V; (f) $I=0.7$ nA, $V=-0.33$ V; (g) $I=0.3$ nA, $V=1$ V; $T=6$ K]. (h) Line profile along the line *C* in (e). The assigned numbers of MLs have been deduced as described in the text. Note that the contrast of the dislocation lines in (e) is reduced with respect to (f) and (g) because of a smaller contrast per ML.

shows a continuous layer where the observable Co steps follow the steps of the W substrate. To illustrate that, the step edges of the underlying W substrate have been identified by the faint height corrugation mentioned previously and are marked as white dashed lines in Figs. 2(e)–2(g). Note that the ten pseudomorphic ML Co film contains only 8.5 closed-packed MLs if one takes into account the relaxation in the different layers described in Sec. III A 1.

3. Dislocation network

As clearly visible in Figs. 2(f) and 2(g) the Co terraces show a periodic zigzag-shaped height modulation consisting of stripes. The stripes run under an angle of $\pm(70° \pm 5°)$ to the $[1\bar{1}0]$ direction of the W(110) substrate, which itself is known from LEED measurements. A closer look at this structure is presented in the constant-current image of Fig. 3(a). It reveals that the stripes consist of two protrusions with different heights, as more clearly visible in the line profile of Fig. 3(b). The higher stripe has a height of 18 ± 7 pm while the shallower one shows a height of only 9 ± 3 pm. The closest distance between shallower and higher stripes is 5 ± 1 nm and thus is approximately one-third of the period of the whole structure of 15 ± 2 nm. However, this period is slightly different in different areas and in some areas, stripes are missing [see Fig. 2(g)]. This results in an average period of 19 nm. Close inspection of Fig. 2(e) reveals that the stripes are also present after annealing at 350 K. However, they appear more irregular and with a lower density than in the film annealed at higher temperatures. The average distance between double stripes is 26 nm for the film annealed at 350 K and 19 nm for the film annealed at 400 K. Further annealing at 450 K has no measurable effect on the stripe density. This implies that the stripe arrangement of Fig. 2(g) is already close to equilibrium.

The stripe-shaped protrusions at the surface most probably originate from dislocation lines (DLs) similar to the dislocation networks found for Cu/Ru(1000),[43,44] Fe/Mo(110),[45,46] Ni/Re(0001),[47] and Ge/Si(111).[48] In these systems the dislocation network is located at the substrate-adsorbate interface, but can still be detected in STM images on up to 10 ML thick films. The corresponding height modulation is of the order of 10 pm. Indeed, it is expected from the strain measurements on Co/W(110) summarized in Sec. III A 1, that misfit dislocations reduce the residual strain above a critical coverage of 10 ML.[29] This is consistent with our observation.

The residual strain in the unrelaxed film would amount to $\varepsilon_x = 3.1\%$ in the $[1\bar{1}0]$ direction (see Sec. III A 1). This means that one additional atomic row oriented along $[001]$ is needed every 32 atomic rows in order to release the stress in the $[1\bar{1}0]$ direction. Since the strained distance of the rows in the $[1\bar{1}0]$ direction is 2.24 Å, this leads to an expected distance between neighboring DLs of 32×2.24 Å $= 7.2$ nm provided that each line contains exactly one additional atom along $[1\bar{1}0]$. Convincingly, this is in good agreement with the measured period of the double stripe structure of 15 ± 2 nm if one assumes that the shallower as well as the higher stripe contain one additional atomic row along $[001]$.

The angle of $\pm 70°$ between DLs and the $[1\bar{1}0]$ direction is probably necessary to simultaneously reduce the residual strain in the $[001]$ direction of $\varepsilon_y = -1.45\%$. To relax this strain, one now has to insert "missing-atom rows" along $[1\bar{1}0]$. Although we could not determine the atomic arrangement which reduces the strain in both directions, it is worth mentioning that the angle $\arctan(|\varepsilon_x/\varepsilon_y|) = 65°$ is indeed close to the observed angle of $70° \pm 5°$. We thus suggest that the stripes are indeed DLs relaxing the stress of the film.

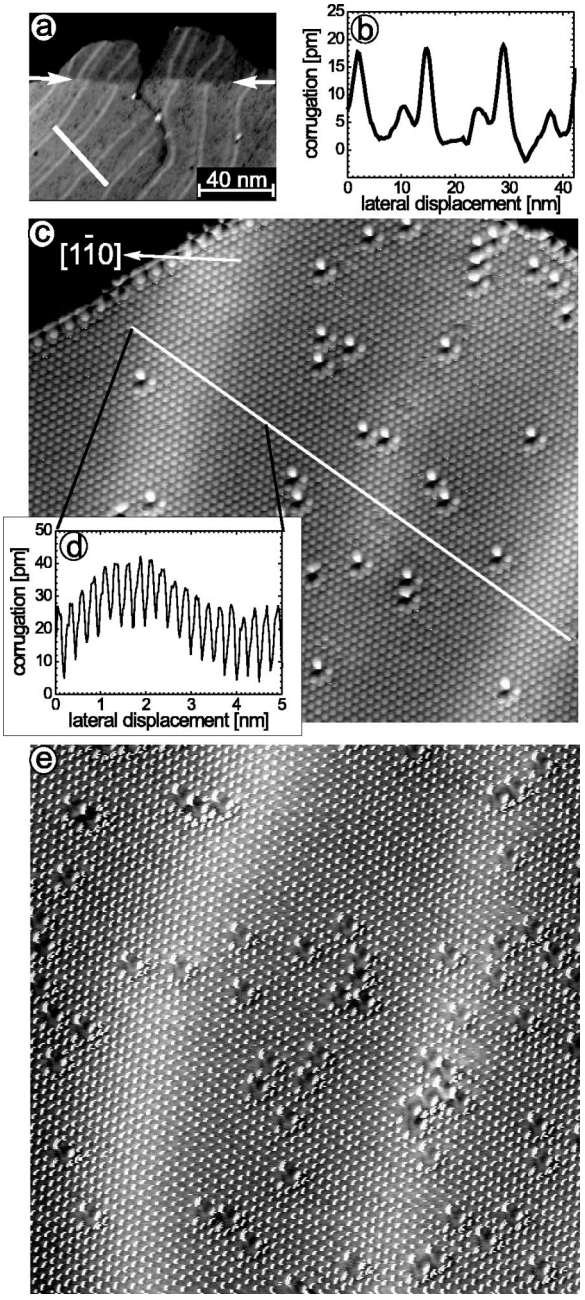

FIG. 3. (a) Constant-current image of the dislocation network across a W step edge on the 10 ML Co film annealed at 400 K ($I = 0.7$ nA, $V = -0.33$ V; $T = 6$ K). The white arrows indicate the underlying W step edge. (b) Line profile along the white line in (a). There are two types of dislocation lines, one appearing as a higher and one as a shallower protrusion. At the underlying W step edge the two types of dislocation lines are interchanged. (c) and (e) Constant-current images with atomic resolution on different terraces of the 10 ML Co film annealed at 350 K [(c) $I = 5$ nA, $V = 10$ mV; (e) $I = 0.9$ nA, $V = 6$ mV; $T = 6$ K]. (d) Line profile along the white line in (c).

In order to prove that the DLs are located close to the interface and not on the surface, Figs. 3(c) and 3(e) show atomically resolved constant-current images taken on two different terraces of the Co film from Fig. 2(e). Besides

2–3% of adsorbate atoms that are imaged as bright dots, the hexagonal Co lattice is clearly visible. From line profiles drawn along the atomic rows as shown in Fig. 3(d), one can deduce a next neighbor distance of 2.65 ± 0.1 Å under an angle of ±30° to the $[1\bar{1}0]$ direction and of 2.5 ± 0.1 Å in the [001] direction. This coincides with the next neighbor distances expected for the Co lattice in the coverage regime 2–10 ML of 2.56 Å and 2.48 Å, respectively (see Sec. III A 1).

More importantly, the stripe-shaped protrusions are also visible in Figs. 3(c) and 3(e), and the atomic resolution reveals that there is no shift in the atomic rows within the stripe structure nor any change in atomic distances on the stripes. This can be clearly seen by inspecting the line profile of Fig. 3(d) and the corresponding line in Fig. 3(c). We conclude that the DLs are not located within the surface layer. Furthermore, the stripe positions are not affected by the Co step edges of the film as can be seen in Figs. 2(e)–2(g), i.e., the direction and height is not changed from one Co layer to the next higher/lower layer. Only at a few step edges adjacent to the two lowest layers in Fig. 2(e) are the stripes disappearing. This means that the DLs are not located in the open four Co layers, but in the first five layers of the Co film next to the W substrate.

In contrast, the step edges of the underlying W substrate have an obvious effect on the stripe structure. In Fig. 3(a) the step edge of the tungsten substrate is visible as a small height change in the Co film (see arrows). At this step, the higher stripe changes into a shallower one and vice versa, i.e., the stripe character is changed at every step edge of the underlying W substrate. Since only the W step edges have an effect on the stripe structure, the most probable position of the DLs is indeed at the Co/W interface in agreement with conventional knowledge on dislocation networks in heterostructures.[43–48] Finally, we should admit that we do not know the origin of the appearance of two different types of DLs. Maybe, the relaxation of a tensile strain in one direction and a compressive strain in the other direction having a ratio of approximately 2:1 requires a network of two different DLs. In any case, the interchange of the DLs at a W step edge is reasonable, since adjacent layers of the W substrate exhibit a corresponding mirror symmetry.

To summarize, we find a dislocation network probably located at the Co/W interface on continuous Co films with 10 ML thickness grown on W(110). This dislocation network is induced by annealing and close to equilibrium above $T\approx400$ K. Surprisingly it consists of two different types of dislocation lines.

B. Spectroscopic results

1. Layer-dependent spectroscopy

Figure 4 shows three spatially averaged dI/dV curves. One is taken on the 10 ML Co film of Fig. 2(g). Another one is taken on monolayer high Co islands of a 0.5 ML film shown in the inset. The last one is recorded on the W substrate visible between the Co islands of the inset. The curve of the 10 ML film shows a sharp peak at −0.3 eV below the Fermi energy. Note that this peak has been found on all

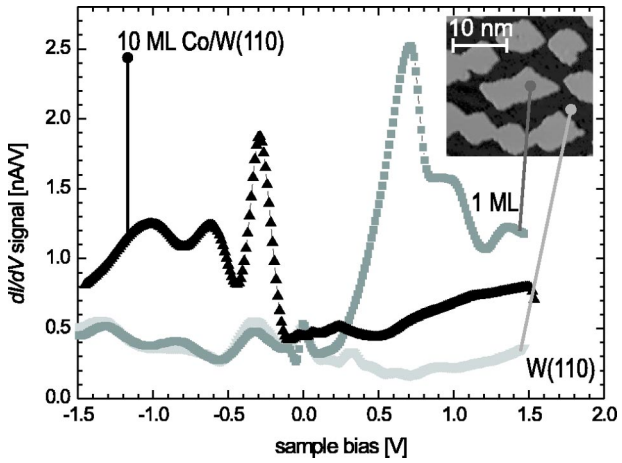

FIG. 4. Spatially averaged dI/dV curve on a 10 ML Co film annealed at 450 K (black curve; $I_{stab}=1$ nA, $V_{stab}=1.5$ V, $V_{mod}=10$ mV) compared to dI/dV curves taken on Co monolayer islands (gray) and on the W(110) substrate (light gray) ($I_{stab}=0.7$ nA, $V_{stab}=-1.5$ V, $V_{mod}=10$ mV). Inset: constant-current image of Co monolayer islands prepared by deposition of 0.5 ML Co on W(110) at room temperature ($I=0.4$ nA, $V=-0.13$ V). Measurement temperature $T=6$ K.

investigated Co films using different tips (PtIr and W). In measurements at room temperature it exhibits a full width at half maximum (FWHM) of 0.35 ± 0.05 eV, while at $T=6$ K a FWHM of 0.2 ± 0.05 eV is observed. Its peak position is at $E-E_F=-0.32\pm0.03$ eV, averaged over eight experiments using three different macrotips. According to this reproducability the peak is caused by an electronic state of the Co sample. In contrast, the other two peaks below E_F at −0.65 eV and −1 eV are either changing their position from tip to tip or are completely absent, making it difficult to identify them as sample states.

The two remaining dI/dV curves in Fig. 4 were taken on Co-ML islands and on the W(110) substrate surrounding the islands. On the Co monolayer the prominent peak has shifted to 0.8 eV above the Fermi energy. On W(110) a rather structureless dI/dV curve is found, as reported previously.[49] A small peak at −0.3 eV is also present in these dI/dV curves but with a much smaller intensity. This underlines that the sharp peak at −0.3 eV is indeed characteristic for the thicker Co films. A similar peak has previously been observed by STS and ARUPS for Co(0001) on various substrates.[8–10,20] In Sec. IV we will show that the peak is assigned to a $d_{3z^2-r^2}$-like surface resonance of a minority-spin character.

To answer the question of whether the position or the intensity of the peak at −0.3 eV depends on the layer thickness of the Co film we took locally resolved dI/dV curves on a wedge-shaped island of a three-dimensional film. The island is shown in Fig. 5(b) and has a 3 ML thickness at the right and an 11 ML thickness at the left rim. The areas of different thickness are visible as ≈5 nm wide stripes separated by darker lines and forming an angle of 30° to the $[1\bar{1}0]$ direction. Additionally, periodic stripes along $[1\bar{1}0]$ with a period of 12.2 ± 0.5 Å are visible on the thin side of the island with a corrugation of ≈5 pm. The latter corrugation is also visible in the line profile of Fig. 5(c). The period

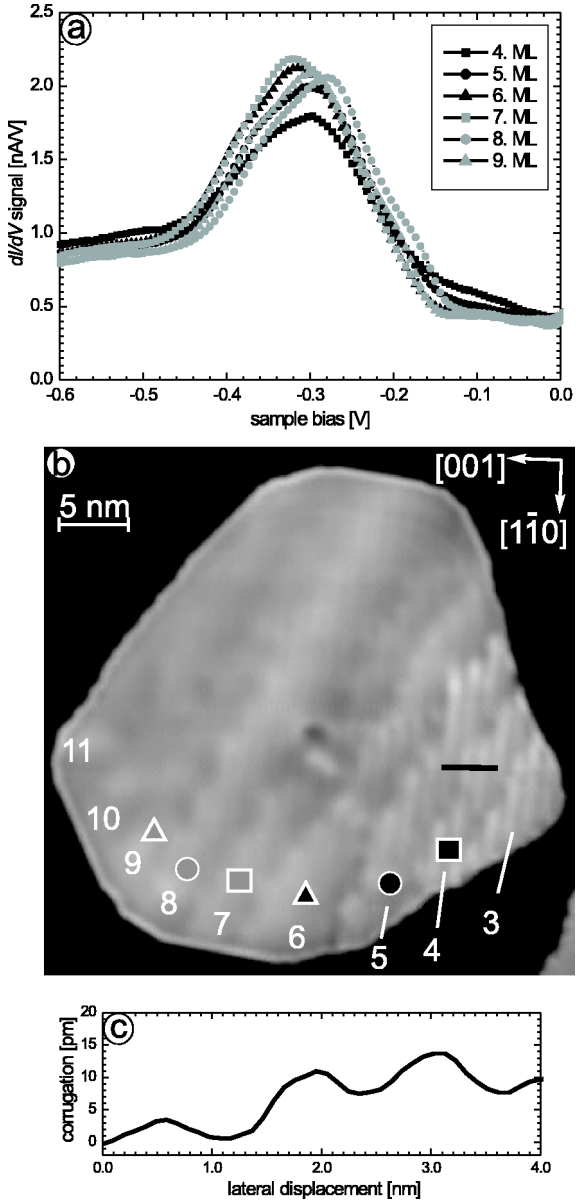

FIG. 5. (a) Spatially averaged dI/dV curves taken on Co layers with increasing thickness as they appear on the island as indicated in (b) (I_{stab}=0.8 nA, V_{stab}=1.5 V, V_{mod}=4 mV). (b) Wedge-shaped Co island of a 3 ML Co film annealed at 500 K. The island is 3 ML thick at the right rim and 11 ML thick at the left rim, as indicated. The step edges of the underlying W substrate are visible as dark stripes running under an angle of 30° to the [1$\bar{1}$0] direction (I =0.5 nA, V=−0.3 V). (c) Line profile along the black line in (b). Measurement temperature T=6 K.

of 12.2 Å can be explained by the (8×1) superstructure or the slightly modified (7.1×1) structure described in Sec. III A 1. If one assumes a simple hard ball model where every fifth Co atom coincides with every fourth W atom along [001], one finds a period of 12.7 Å for the (8×1) structure. For the (7.1×1) structure the strain is reduced by 2.45% (see Sec. III A 1) leading to a period of 12.4 Å. Indeed, a similar appearance of such a superstructure in STM images has previously been observed on 1 ML high films of Co and Ni on W(110).[30,50] We find that the corrugation decreases with increasing film thickness being less than 1 pm above 6 ML.

Figure 5(a) shows dI/dV curves recorded on the areas of different thickness. A peak at −0.3 eV is clearly visible at each thickness. From layer to layer the peak energy shifts by as little as ±0.02 eV. Defining a contrast of the peak intensity by

$$C_{a,b}=\frac{(dI/dV)_a-(dI/dV)_b}{[(dI/dV)_a+(dI/dV)_b]/2}, \tag{2}$$

where a and b denote the number of layers, we find a maximum contrast of only $C_{4,7}$=20%. Above the fifth monolayer, the contrast $C_{a,b}$ is even less than 10%. This means that regarding the electronic properties, the fifth monolayer is already bulklike as has previously been found on continuous films by ARUPS.[13] The larger contrast from the fourth to the fifth monolayer can possibly be attributed to the larger influence of strain at this thickness.

2. Oxygen adsorption

In order to find out how sensitive the peak at −0.3 eV reacts upon changes at the surface we exposed the Co islands from Fig. 5(b) to an oxygen amount of 2.2 L O_2 (1 L=10^{-6} Torr s). Since sticking coefficients of O on W(110) are measured to be in the range of 0.3–0.6 (Refs. 51,52) and since it is known that O_2 adsorbs dissociatively on Co(0001) (Ref. 53) the oxygen exposure of 2.2 L O_2 results in a coverage of 20% to 40% O atoms per Co unit cell. The constant-current image after exposure is shown in Fig. 6(b). It shows depressions that have a depth of 60–80 pm as visible in the line profile in Fig. 6(c). The depressions cover approximately 20% of the island surface. We therefore conclude that these depressed areas correspond to the O atoms whereas the rest of the surface is clean Co. Indeed oxygen adsorbates are known to be imaged as depressions in constant-current images on many metal surfaces.[54,55]

We now aquired dI/dV curves on the oxygen areas and on the neighboring Co areas. The curves are shown in Fig. 6(a) in comparison with a curve obtained on the Co island prior to O_2 dosage. The Co areas after O_2 dosage still show a peak close to −0.3 eV, which is only slightly decreased in intensity by $C_{OCo,Co}$=−10%. In contrast, on the oxygen-covered areas the peak has completely vanished. The corresponding state consequently reacts extremely sensitively on adsorbates. This has also been shown by hydrogen exposure on Co(0001) in an early ARUPS study.[20] As usual, we conclude that the peak at −0.3 eV is either induced by a surface state or by a surface resonance. Our spatially resolved spectroscopy study shows in addition that the quenching of the state is restricted to the very surrounding of the oxygen, which indicates a rather local character of the corresponding state.

3. Spatially resolved spectroscopy

To find out the spatial distribution of the peak at −0.3 eV we performed dI/dV maps at the peak position as shown in Fig. 7. For both the islands shown in Figs. 7(a)–7(d) and the continuous film shown in Figs. 7(e) and 7(f), a fraction of the

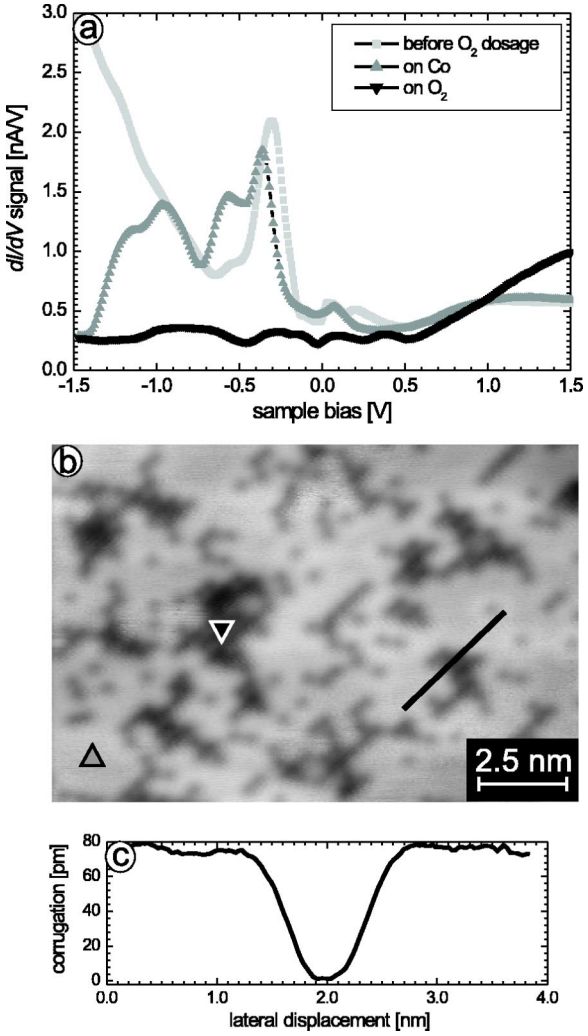

FIG. 6. (a) Spatially averaged dI/dV curves taken before (light gray) and after the exposure of the Co film from Fig. 5(b) to 2.2 L O_2 ($I_{stab}=0.8$ nA, $V_{stab}=1.5$ V, $V_{mod}=20$ mV). The dI/dV curves after dosage are taken on the uncovered Co areas (gray triangles) and on the O_2 covered areas (black upside-down triangles), as indicated in (b). (b) Constant-current image of the Co-island surface after O_2 dosage ($I=0.4$ nA, $V=-0.3$ V). (c) Line profile along the black line in (b). Measurement temperature $T=6$ K.

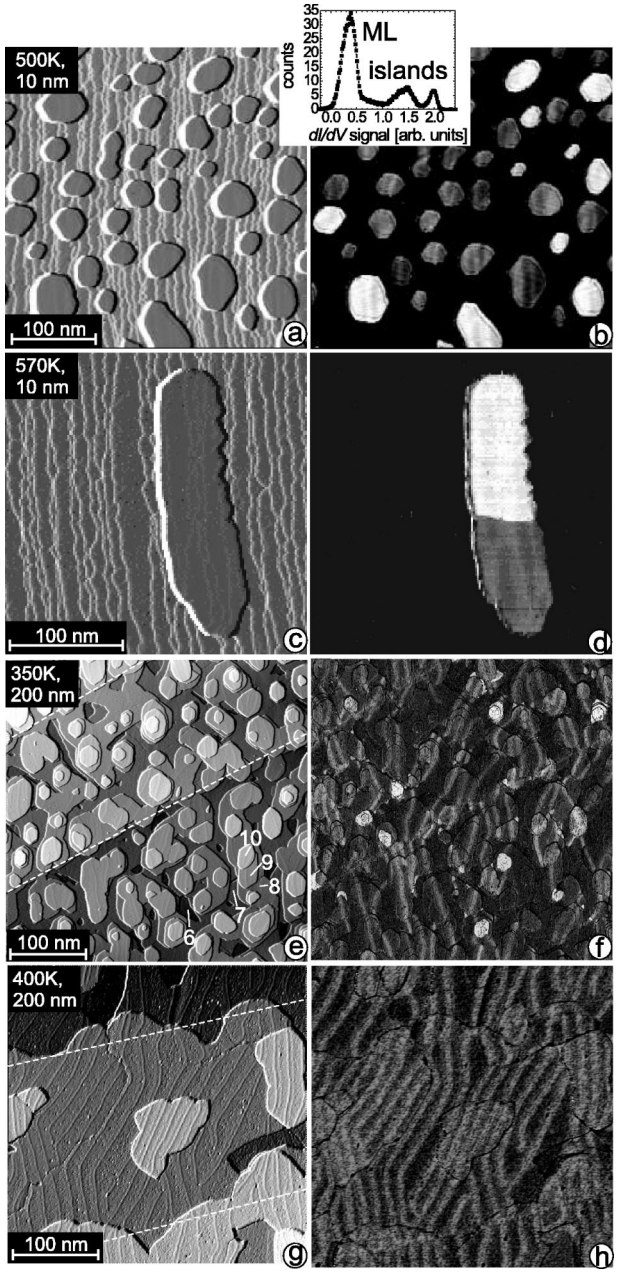

FIG. 7. Constant-current images (left panels) and corresponding dI/dV maps (right panels) of the same sample area of different Co films. Terrace width of the W(110) substrate and annealing temperature are indicated in the upper left corners. (a) and (b) 3 ML Co film ($I_{stab}=0.3$ nA, $V_{stab}=-0.3$ V, $V_{mod}=30$ mV, $T=300$ K). Inset: histogram of dI/dV values from (b). (c) and (d) 2 ML Co film. The island is 4 ML thick at the right and 12 ML thick at the left rim and shows a dI/dV contrast on its atomically flat surface ($I_{stab}=0.4$ nA, $V_{stab}=-0.3$ V, $V_{mod}=30$ mV, $T=300$ K). (e) and (f) 10 ML Co film. The numbers mark the local Co thickness in ML. (g) and (h) 10 ML Co film ($I_{stab}=0.7$ nA, $V_{stab}=-0.33$ V, $V_{mod}=20$ mV, $T=6$ K). The dashed white lines in (e) and (g) mark the step edges of the underlying W substrate.

dI/dV maps appears brighter than the surroundings. A histogram of dI/dV values shown in the inset of Fig. 7(b) reveals that the dI/dV distribution on the Co islands is bimodal, i.e., there is a large peak that originates from the Co ML between the islands and two smaller peaks correspond to the dI/dV intensity on the islands. This implies that there are two spectroscopically distinct island types. One has a larger and the other a smaller dI/dV signal at −0.3 eV. The same conclusion can be drawn for the continuous film in Fig. 7(f), where a few bright terraces appear among the majority of darker terraces. The less bright stripe-shaped areas, that are also visible in Fig. 7(h), are caused by the DLs and will be discussed later. The dI/dV contrast between dark (d) and bright (b) areas is $C_{b,d}=40\pm20\%$ according to Eq. (2). This contrast is found for both morphologies, islands and continuous films. It does not depend systematically on the temperature at

which spectroscopy is performed. Since $C_{b,d}$ is considerably larger than the thickness-induced contrast discussed in Sec. III B 1, the dark and bright areas are not an effect of the film thickness.

Next, we analyze the spatial distribution and the relative frequency of the bright and dark areas. From Fig. 7(b) it is obvious that individual islands mostly have a single brightness, i.e., they are either completely dark or completely bright. Only larger islands such as the one in Figs. 7(d) exhibit a contrast change within the island. Moreover, it is obvious that the bright areas appear more often in the island morphology than in the continuous film. Indeed, the continuous film of Fig. 7(h) does not show any bright areas within the image range. A quantitative analysis reveals that in the films with island morphology in Figs. 7(b) and 7(d) the bright areas take $25\pm5\%$ of the island surface, while the continuous films in Figs. 7(f) and 7(h) exhibit only $3\pm1\%$ and 0% of bright areas, respectively.

Figure 8(a) shows local dI/dV curves taken on the bright and dark areas of Fig. 8(e) as indicated. The spectroscopic difference between the bright and dark areas is visible as a different intensity of the peak at -0.3 eV, while the peak position is only slightly changed between the curves. Contrasts in peak intensity ranging from $C_{b,d}=30\%$ to $C_{b,d}=70\%$ are found in different measurement sets obtained after preparing different microtips. However, the contrast does not depend systematically on the growth morphology or on the measurement temperature. Thus, we attribute the variance in contrasts to a different density of states of the microtip.[32–34] The second spectroscopic difference between bright and dark areas is a small but systematic downward shift of the peak position on the bright areas by 55 ± 35 meV. Note finally that the dI/dV intensity *above* E_F is basically the same in all three curves in contrast to previous measurements on Co/Cu(111).[7]

The question arises about what could be the reason for the spectroscopic difference of bright and dark areas. In Sec. III B 1 we have shown that the effect of layer thickness on the peak height is less than 10%, which is considerably smaller than the contrast between bright and dark areas. It is also unlikely that residual gas adsorption is the reason for the spectroscopic difference. As shown in Sec. III B 2 the peak intensity changes by only $C_{OCo,Co}=-10\%$ on the oxygen-free areas of Co when 20% of the Co film is covered with oxygen. In contrast, even though the film as prepared in Figs. 8(b)–8(e) shows an adsorbate coverage of only 1% in the bright areas and 5% in the dark areas, the contrast between the areas is as large as 50%. Furthermore, we can exclude that a different atomic surface structure of bright and dark terraces is responsible for the contrast. The atomically resolved constant-current images of Figs. 3(c) and 3(e) are recorded on a bright area and a dark area, respectively. Nevertheless, we find exactly the same hexagonal arrangement of Co atoms.

Since it has previously been shown that stacking can be a source of dI/dV contrast on Co and Gd,[7,8,56] we finally check this assumption. A close inspection of Figs. 8(b) and 8(c) shows indeed that different stacking leads to a contrast change. The figure shows two islands of monolayer height placed on the same Co terrace. Both islands are hexagonal

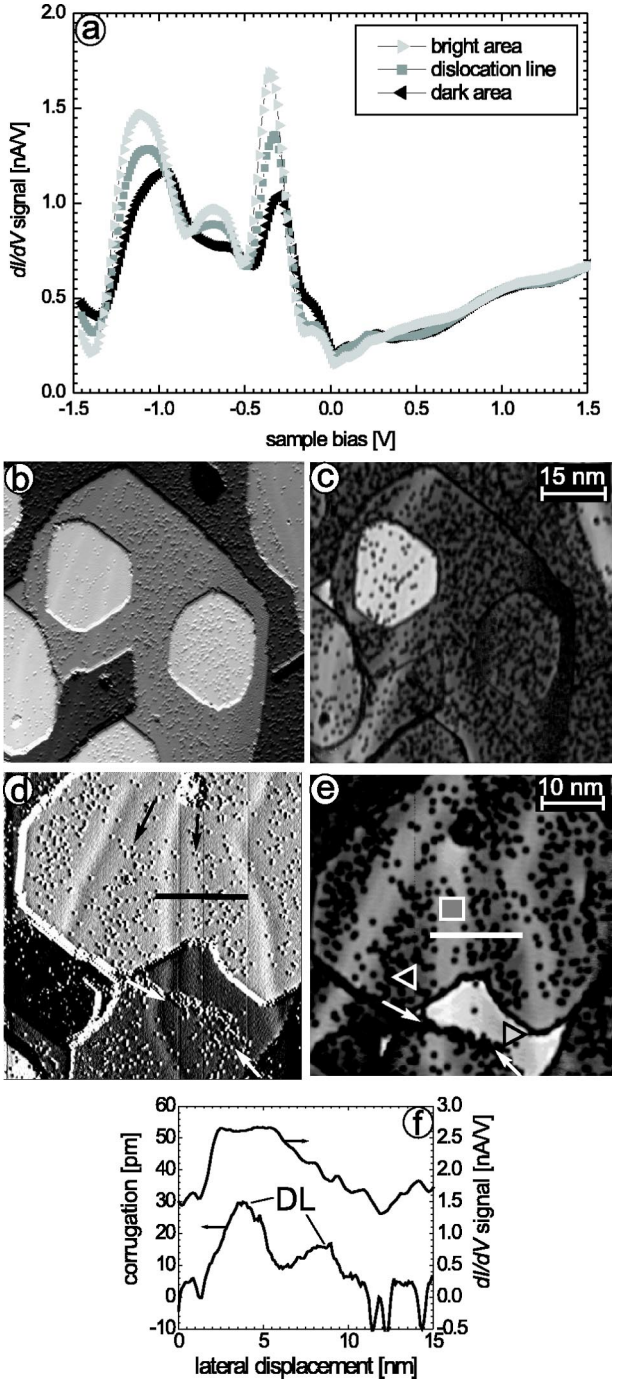

FIG. 8. (a) Spatially resolved dI/dV curves taken on the bright and the dark Co islands and on the dislocation lines from a 10 ML Co film annealed at 350 K ($I_{stab}=0.7$ nA, $V_{stab}=1.5$ V, $V_{mod}=10$ mV). The origin of the curves is marked in (e). (b)–(e) Constant-current images (left panels) and corresponding dI/dV maps of the same sample area (right panels) of two regions of the Co film ($I_{stab}=0.7$ nA, $V_{stab}=-0.33$ V, $V_{mod}=20$ mV). (b) and (c) shows two adjacent monolayer high fcc- and hcp-stacked islands on the same Co terrace. White arrows in (d) and (e) mark a contrast change in the same atomic layer. Black arrows in (d) mark two shallow dislocation lines. (f) Line profiles drawn along the black and white lines in (d) and (e), respectively, at the same position. Dislocation lines are marked. Measurement temperature $T=6$ K.

with three shorter and three longer step edges. However, the short and long step edges are interchanged between the two islands, i.e., the left island reminds us of a right-pointing triangle, whereas the right island reminds us of a left-pointing triangle. This indicates different stacking as discussed, e.g., by Busse *et al.*[57] Stackings can be multifold in 10 ML thick films but the upper three layers they can only be *ABA* or *ABC*, corresponding to an hcp- or an fcc-like stacking, respectively. So, we identify the two islands as *ABA* and *ABC* stacked. Spectroscopically, the right island appears dark in Fig. 8(c), while the left island appears bright with a contrast of $C_{b,d}=60\%$. This strongly implies that stacking is the origin of the observed bimodal contrast.[58] Since it is, moreover, known that Co films on W(110) are predominantly hcp stacked,[13] it is straightforward to identify the more frequent dark areas with *ABA* stacking and the less frequent bright areas with *ABC* stacking.

An example where fcc and hcp stacking is found within the same island is shown in Figs. 8(d) and 8(e). The bright area is adjacent to a dark area on the same atomic layer where the boundary is indicated by white arrows. Moreover, a dark area is one monoatomic layer on top of the bright area. This indicates a burried stacking fault with the stacking sequence of the top layer *B* being *ABCB*.

In summary, all found bright areas are consistent with an fcc-like stacking appearing exactly at this layer. We conclude that the peak at −0.3 eV exhibits an intensity change of about +50% and a peak shift of −55 meV at a fcc-stacking fault. Moreover, we conclude that while hcp stacking is nearly exclusive in continuous films, a significant tendency to fcc stacking appears on Co islands.

Let us come back to the less bright, stripe-shaped areas visible in the dI/dV maps of Figs. 7(f) and 7(h). By comparison with the corresponding constant-current images in Figs. 7(e) and 7(g) it is clear that this contrast is caused by the DLs discribed in Sec. III A 3. Note that it is hard to distinguish the shallower and the higher DL in the dI/dV maps as can be seen in the line profiles of Fig. 8(f). The double line consisting of a shallower and a higher DL appears as a broad asymmetric single stripe in the dI/dV signal. Local spectroscopy on the double line as shown in Fig. 8(a) reveals that again the intensity of the peak at −0.3 eV is responsible for the contrast. The peak intensity on the double line is by $C_{DL,hcp}=25\pm15\%$ higher than on the surrounding hcp areas and the peak shifts downwards by 40 ± 10 meV. Interestingly, the DLs are also brighter than their surroundings on fcc-stacked areas as can be seen on the bright area in Fig. 8(e). Although we currently do not know the origin of the contrast on the DLs, it is likely that the long-range strain field has a strong influence on the peak intensity, as will be confirmed in the next section.

IV. CALCULATIONS

In order to find the reason for the intensity change of the peak at −0.3 eV on fcc-stacking faults, we performed density-functional theory (DFT) calculations.[59] The exchange-correlation functional is formulated within the generalized gradient approximation.[60] The Kohn-Sham equations are solved applying the full-potential linearized plane-wave (FLAPW) method, as realized in the FLEUR code.[61,62] For simulating the Co(0001) surface we use a film geometry with 12 layers of Co embedded in infinite vacua on both sides of the film. We compare the perfect hcp structure (*ABA*) with an hcp structure exhibiting an fcc stacking-fault (*ABC*) in both surface layers. Both geometries are optimized by total-energy minimization using the theoretical Co bulk lattice constant, which is determined to 2.509 Å (experimental value 2.507 Å). Self-consistent results have been obtained with about 110 basis functions per atom and 26 **k** points in the irreducible wedge of the two-dimensional Brillouin zone (2DBZ) as numerical parameters. For the calculation of the density of states (DOS) we used 50 **k** points in the irreducible wedge of the 2DBZ.

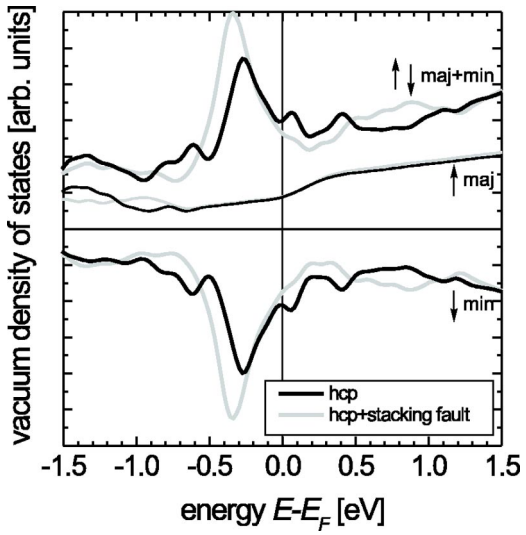

FIG. 9. The calculated vacuum DOS of the unfaulted structure (black) and of the faulted structure (gray) of a 12 ML Co film at a distance of 3 Å from the surface layer. Maj, min, and maj + min indicate the majority DOS, the minority DOS, and the sum of both, respectively. All curves are shown on the same scale.

Compared with the ideal bulk termination, both surfaces are relaxed inwards. The surface layer of the faulted structure is relaxed by 0.046 Å and that of the unfaulted structure by 0.015 Å, which corresponds to 2.3% and 0.7% of the Co interlayer distance of 2.034 Å, respectively. The work functions of the faulted and the unfaulted structure are nearly identical, i.e., 5.143 and 5.096 eV, respectively. Thus, the decay constants of the wave functions into the vacuum are comparable.

To simulate the spectroscopic measurements we calculated the vacuum DOS for both structures. The energies are given with respect to the Fermi level. Since the work functions of the faulted and the unfaulted structure differ by 47 meV, the Fermi levels are shifted accordingly with respect to the vacuum zero. The results for majority-spin DOS and minority-spin DOS, as well as the sum of both DOSs, are presented in Fig. 9 at a distance of 3 Å from the surface layer. We find a dominating peak in the minority-spin DOS at approximately −0.3 eV below E_F exhibiting a FWHM of 0.3 ± 0.05 eV. Since the proportion between different peaks

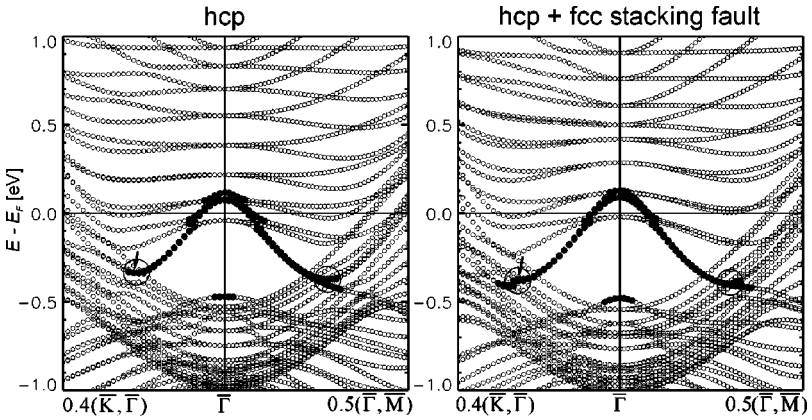

FIG. 10. The minority-spin band structure of the 12 ML Co film in the unfaulted (left panel) and in the faulted (right panel) structure are plotted along the high symmetry directions in the neighborhood of $\bar{\Gamma}$. Black dots mark states that are localized to more than 10% in vacuum. The larger circles mark the band minimum region (see text). The state used for the contour plots in Fig. 11 is indicated with an arrow.

in the vacuum DOS can change with the distance from the surface, we checked the vacuum DOS at distances ranging from 2–10 Å. For these distances the peak at −0.3 eV remains the dominating feature for both structures. Consequently, this peak corresponds to the one found in STS measurements.

As visible in Fig. 9, the faulted structure (f) exhibits a higher peak intensity than the unfaulted structure (u). According to Eq. (2) the contrast amounts to $C_{f,u}=30\%$ at 2–3 Å distance, but decreases to $C_{f,u}=5\%$ at 10 Å distance. Moreover, the peak on the faulted structure is at −0.34 eV, while that on the unfaulted structure is at −0.28 eV. This means that the peak on the faulted structure is shifted by 60 meV to lower energies. Both results are in excellent agreement with the STS results where an intensity change of $(50\pm20)\%$ and an energy shift of 55 ± 35 meV are found. Finally, the calculated peak width is in reasonable agreement with the experimental result.

Next we want to understand the mechanism of why fcc stacking leads to a higher peak intensity. To answer this question, we first compare the vacuum DOS with the band structures of faulted and unfaulted surfaces. Figure 10 shows band structures of the minority spin for both systems along the high symmetry directions. States, which have more than 10% of their DOS in vacuum, are marked by black dots. The corresponding bands are identified as surface-related bands. One of those bands[63] exists in the energy range corresponding to the peak at −0.3 eV. It has a minimum marked by the circles in Fig. 10 at approximately one fourth of the distance from $\bar{\Gamma}$ to $\bar{K}$ and from $\bar{\Gamma}$ to $\bar{M}$, respectively. This minimum is close to −0.3 eV. We checked that the main contribution to the vacuum DOS comes indeed from this band minimum. A second surface band has a maximum at about −0.5 eV and is located at the $\bar{\Gamma}$ point. The contribution of this band to the peak at −0.3 eV in the vacuum DOS is negligible, since the band maximum occurs at lower energies. In fact, we find that the contribution from $\bar{\Gamma}$ to the peak is a factor of 10 lower than the contribution from the band minimum off from $\bar{\Gamma}$. Consequently the peak at −0.3 eV is caused by the band minimum of the surface band at 1/4 of the 2DBZ. We conclude that this band minimum is the origin of the peak measured by STS. This is in contrast to conclusions given for Co/Cu(111), where a band at $\bar{\Gamma}$ has been proposed to be responsible for the peak.[9,10] Note that the band maximum at $\bar{\Gamma}$ is isolated from other bulk bands and is, thus, a surface *state*. In contrast, the band minimum at 1/4 of the 2DBZ crosses other bulk bands and is, thus, probably a surface *resonance*.

Finally, we analyze the charge distribution of the surface bands. The character of the band with the minimum at 1/4 of the 2DBZ changes from the band maximum at $\bar{\Gamma}$, where it has a predominant p character, to the band minimum, where it has a $d_{3z^2-r^2}$ character with a small contribution of s and p states of less than 5%. This is shown in Fig. 11, where contour plots of the minority spin density at the energy and Bloch vector corresponding to the band minimum marked by arrows in Fig. 10 are given. For faulted and unfaulted struc-

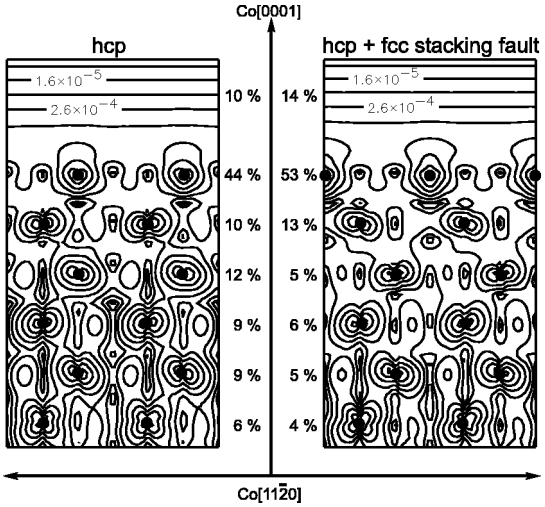

FIG. 11. Contour plots of the spin density of the minority electrons for the state marked with an arrow in Fig. 10 for the 12 ML Co film in the unfaulted (left panel) and in the faulted (right panel) structure. The numbers marking the contour lines give the corresponding charge density in electrons/(a.u.)^3. Two successive lines differ by a factor of 4. Crystallographic directions of the Co(0001) lattice are indicated. The black dots mark the positions of the closest atoms projected onto the plane. The numbers beside the contour plots give the contribution of the state to the LDOS in percent for this layer or vacuum, normalized to six layers. They are obtained by integrating over the muffin tins in each layer and over the vacuum, respectively.

ture the contour plots show a predominant $d_{3z^2-r^2}$ character at the surface layer with a minor superposition of an *s*-like character. Within the bulk, the LDOS has predominant d_{xz} character. The contribution of this particular state to the LDOS in each layer and in vacuum is indicated by the numbers next to the contour plots. Obviously, the largest contribution is in the surface layer. Nevertheless, there is a considerable contribution in the subsurface layers. This means that the state at the surface can couple to bulk *d* states. That this coupling takes place indeed can be concluded from the hybridization with the bulk *d* bands near the band minimum, which is marked in Fig. 10. Consequently, the state has to be assigned to a surface *resonance* rather than to a surface *state*. In contrast, the dot-marked band with the maximum at −0.5 eV at $\bar{\Gamma}$ is found to be a $d_{3z^2-r^2}$-surface *state* (not shown) in accordance with the Co/Cu(111) case.[9,10]

The contour plots in Fig. 11 also show that in the case of hcp stacking the downward oriented lobes of the surface atoms point directly to the atoms in the second subsurface layer. In contrast, in the case of the faulted structure, the lobes point into the interstitial region. Accordingly, the surface resonance exhibits a stronger coupling to bulk *d* states at pure hcp stacking than at stacking faults. This leads to a weaker localization in the surface layer in the hcp case as can also be seen by comparing the distribution of the LDOS in the different layers (Fig. 11). As a consequence, the intensity of the vacuum DOS as measured by STS is lower for the hcp structure. The reason for a different brightness of hcp and fcc areas in dI/dV maps at −0.3 eV is, thus, a different coupling of the $d_{3z^2-r^2}$-like surface resonance to the underlying bulk. Note that the intensity of the surface resonance in the hcp case is larger in the second subsurface layer than in the first subsurface layer. This stresses that the geometrically induced coupling to the second subsurface layer is indeed the relevant coupling. Furthermore, we want to point out that, in the hcp case, the surface resonance crosses only one bulk *d* band in the $(\bar{\Gamma},\bar{K})$ direction before it runs into the band minimum. In contrast, in the case of fcc stacking, the surface resonance crosses two bulk *d* bands. Since the *d* band to which the band minimum couples is approximately 50 meV lower in energy in the fcc case, the peak in the vacuum DOS accordingly occurs at lower energies.

We did not yet analyze in detail the mechanism that leads to a higher intensity in the vacuum DOS of the surface resonance at DLs. Probably, the lateral extension of the lattice at DLs arising together with the vertical compression leads to an increase in intensity. Indeed our calculations using different lattice parameters suggest that the intensity of the peak at −0.3 eV is increased by stretching the Co(0001) structure. However, this effect has to compensate the opposite one given by the vertical compression.

In summary, the peak at −0.3 eV measured by STS is assigned to a $d_{3z^2-r^2}$-like surface resonance with a minority-spin character that is located in a band minimum *off* from $\bar{\Gamma}$. In contradiction, for the case of Co/Cu(111), Diekhöner *et al.*[9] and Okuno *et al.*[10] assigned the peak to a $d_{3z^2-r^2}$-surface state *at* $\bar{\Gamma}$. More importantly, we identified the different appearance of hcp- and fcc-stacked areas in dI/dV maps as due to a different coupling of the corresponding surface resonance to the bulk.

Finally we want to point out that the total energy of the faulted structure (fcc) is only 11 meV/atom larger than that of the unfaulted structure (hcp). This suggests that stacking fault nucleation sites occur rather frequently in thin film growth,[57] possibly explaining our observation that fcc areas exist in thin films even at room temperature.

V. CONCLUSIONS

In summary, we have investigated the electronic structure of the Co(0001) surface on islands and continuous films grown on W(110) by STS. On both, we found a surface-related peak at −0.3 eV below the Fermi energy. By first-principles electronic structure calculations this peak is assigned to a $d_{3z^2-r^2}$-like surface resonance with a minority-spin character. It belongs to a band minimum at 1/4 of the two-dimensional Brillouin zone away from $\bar{\Gamma}$. STS reveals that the surface resonance is extremely sensitive to stacking as well as to the strain field of dislocation lines. According to the calculations, fcc stacking at the surface results in an increase of the vacuum density of states by 5–30%, depending on the tip-sample distance, while STS experiments find an increase of (50±20)%. The different intensity is caused by a different coupling strength of the surface resonance to bulk states for fcc and hcp stacking leading to a different localization in the surface layer and, thus, to a different dI/dV signal. Although a contrast in dI/dV on different stackings has also been found in the Co/Cu(111) system by Vázques de Parga *et al.*,[7] it has been attributed to a peak above E_F, which is at variance with the peak measured on the same system by Pietzsch *et al.*,[8] Diekhöner *et al.*[9] and Okuno *et al.*[10] Since Vázques de Parga *et al.* do not find a feature in the energy range of the surface resonance, one possible explanation for their results could be intermixing or contamination leading to a change in electronic structure. However, since our explanation for the contrast in dI/dV on different stackings is based on the commonly measured peak on both Co systems, we believe that our results are generally correct for clean Co(0001).

Finally, we found that the film morphology is important for the stacking, i.e., fcc stacking appears to be considerably increased in Co islands compared to continuous Co films. This effect should be considered with respect to nanostructuring of magnetic multilayers. Since the observed surface resonance exhibits a spin polarization of 70%, interesting future experiments using spin-polarized STS can be anticipated.

Note added in proof: Recently, we have become aware of a similar observation for the low coverage regime of Co/W(110).[64]

ACKNOWLEDGMENTS

We thank E. Konenkova and F. Meier for assisting during the measurements and we acknowledge financial support from SFB 508-B4 and Graduiertenkolleg "Physik nanostrukturierter Festkörper" of the "Deutsche Forschungsgemeinschaft."

*Author to whom correspondence should be sent. Electronic address: jwiebe@physnet.uni-hamburg.de
†Present address: Department of Physics, University of California at Berkeley, Berkeley, California 94720-7300.
‡http://www.nanoscience.de/group_r/

[1] G. Prinz, Science **282**, 1660 (1998).
[2] S. Parkin, Phys. Rev. Lett. **71**, 1641 (1993).
[3] P. Zahn, J. Binder, I. Mertig, R. Zeller, and P. H. Dederichs, Phys. Rev. Lett. **80**, 4309 (1998).
[4] E. B. Myers, D. C. Ralph, J. A. Katine, R. N. Louie, and R. A. Buhrman, Science **285**, 867 (1999).
[5] J. M. De Teresa, A. Bartélémy, A. Fert, J. P. Contour, R. Lyonnet, F. Montaigne, P. Seneor, and A. Vaurès, Phys. Rev. Lett. **82**, 4288 (1999).
[6] J. M. De Teresa, A. Bartélémy, A. Fert, J. P. Contour, F. Montaigne, and P. Seneor, Science **286**, 507 (1999).
[7] A. L. Vázques de Parga, F. J. García-Vidal, and R. Miranda, Phys. Rev. Lett. **85**, 4365 (2000).
[8] O. Pietzsch, A. Kubetzka, M. Bode, and R. Wiesendanger, Phys. Rev. Lett. **92**, 057202 (2004).
[9] L. Diekhöner, M. A. Schneider, A. N. Baranov, V. S. Stepanyuk, P. Bruno, and K. Kern, Phys. Rev. Lett. **90**, 236801 (2003).
[10] S. N. Okuno, T. Kishi, and K. Tanaka, Phys. Rev. Lett. **88**, 066803 (2002).
[11] J. de la Figuera, J. E. Prieto, C. Ocal, and R. Miranda, Surf. Sci. **307**, 538 (1994).
[12] A. Rabe, N. Memmel, A. Steltenpohl, and T. Fauster, Phys. Rev. Lett. **73**, 2728 (1994).
[13] H. Knoppe and E. Bauer, Phys. Rev. B **48**, 1794 (1993).
[14] J. Bansmann, M. Getzlaff, and G. Schönhense, J. Magn. Magn. Mater. **148**, 60 (1995).
[15] M. Getzlaff, J. Bansmann, J. Braun, and G. Schönhense, J. Magn. Magn. Mater. **161**, 70 (1996).
[16] J. Bansmann, L. Lu, M. Getzlaff, M. Fluchtmann, J. Braun, and K. H. Meiwes-Broer, J. Magn. Magn. Mater. **185**, 94 (1998).
[17] J. Bansmann, L. Lu, V. Senz, A. Bettac, M. Getzlaff, and K. W. Meiwes-Broer, Eur. Phys. J. D **9**, 461 (1999).
[18] J. Bansmann, L. Lu, M. Getzlaff, M. Fluchtmann, and J. Braun, Surf. Sci. **454**, 686 (2000).
[19] C. Math, J. Braun, and M. Donath, Surf. Sci. **482–485**, 556 (2001).
[20] F. J. Himpsel and D. E. Eastman, Phys. Rev. B **20**, 3217 (1979).
[21] E. Wetli, T. J. Kreutz, H. Schmid, T. Greber, J. Osterwalder, and M. Hochstrasser, Surf. Sci. **402–404**, 551 (1998).
[22] J. Braun and M. Donath, Europhys. Lett. **59**, 592 (2002).
[23] C. Wittneven, R. Dombrowski, S. H. Pan, and R. Wiesendanger, Rev. Sci. Instrum. **68**, 3806 (1997).
[24] J. Wiebe, Ph.D. thesis, Institute of Applied Physics, University of Hamburg, 2003.
[25] A. Wachowiak, Ph.D. thesis, Institute of Applied Physics, University of Hamburg, 2003.
[26] M. Bode, R. Pascal, and R. Wiesendanger, Surf. Sci. **344**, 185 (1995).
[27] B. G. Johnson, P. J. Berlowitz, D. W. Goodman, and C. H. Bartholomew, Surf. Sci. **217**, 13 (1989).
[28] J. G. Ociepa, P. J. Schultz, K. Griffiths, and P. Norton, Surf. Sci. **225**, 281 (1990).
[29] H. Fritzsche, J. Kohlhepp, and U. Gradmann, Phys. Rev. B **51**, 15933 (1995).
[30] M. Pratzer, H. Elmers, and M. Getzlaff, Phys. Rev. B **67**, 153405 (1998).
[31] J. Klijn, L. Sacharow, Chr. Meyer, S. Blügel, M. Morgenstern, and R. Wiesendanger, Phys. Rev. B **68**, 205327 (2003).
[32] J. Tersoff and D. R. Hamann, Phys. Rev. Lett. **50**, 1998 (1983).
[33] J. Tersoff and D. R. Hamann, Phys. Rev. B **31**, 805 (1985).
[34] M. Morgenstern, D. Haude, V. Gudmundsson, C. Wittneven, R. Dombrowski, C. Steinebach, and R. Wiesendanger, J. Electron Spectrosc. Relat. Phenom. **109**, 127 (2000).
[35] A. Bauer, A. Mühlig, T. Günther, M. Farle, K. Baberschke, and G. Kaindl, Morphology and Curie Temperature Changes upon Annealing of Co/W(110), Mater. Res. Soc. Symp. Proc. No. 475 (Materials Research Society, Pittsburgh, 1997), p. 27.
[36] G. Garreau, M. Farle, E. Beaupaire, and K. Baberschke, Phys. Rev. B **55**, 330 (1997).
[37] *Handbook of Chemistry and Physics*, edited by R. C. Weast (CRC, Boca Raton, FL, 1989).
[38] S. Müller, G. Kostka, T. Schäfer, J. de la Figuera, J. E. Prieto, C. Ocal, R. Miranda, K. Heinz, and K. Müller, Surf. Sci. **352**, 46 (1996).
[39] A. Atrei, G. Rovida, M. Torrini, U. Bardi, M. Gleeson, and C. J. Barnes, Surf. Sci. **372**, 91 (1997).
[40] E. Bauer, private communication.
[41] R. Pascal, C. Zarnitz, M. Bode, M. Getzlaff, and R. Wiesendanger, Appl. Phys. A: Mater. Sci. Process. **65**, 603 (1997).
[42] A. Wachowiak, J. Wiebe, M. Bode, O. Pietzsch, M. Morgenstern, and R. Wiesendanger, Science **298**, 577 (2002).
[43] J. C. Hamilton and S. M. Foiles, Phys. Rev. Lett. **75**, 882 (1995).
[44] J. de la Figuera, A. K. Schmid, N. C. Bartelt, K. Pohl, and R. Q. Hwang, Phys. Rev. B **63**, 165431 (2001).
[45] J. Malzbender, M. Przybylski, J. Giergel, and J. Kirschner, Surf. Sci. **414**, 187 (1998).
[46] S. Murphy, D. Mac Mathúna, G. Mariotto, and I. V. Shvets, Phys. Rev. B **66**, 195417 (2002).
[47] M. Stindtmann, M. Farle, T. S. Rahman, L. Benabid, and K. Baberschke, Surf. Sci. **381**, 12 (1997).
[48] B. Voigtländer and N. Theuerkauf, Surf. Sci. **461**, L575 (2000).
[49] M. Bode, R. Pascal, and R. Wiesendanger, J. Vac. Sci. Technol. A **15**, 1285 (1997).
[50] D. Sander, C. Schmidthals, A. Enders, and J. Kirschner, Phys. Rev. B **57**, 1406 (1998).
[51] M. E. Bride and R. M. Lambert, Surf. Sci. **82**, 413 (1979).
[52] G. R. Castro and J. Kuppers, Surf. Sci. **123**, 456 (1982).
[53] M. Getzlaff, J. Bansmann, and G. Schönhense, J. Magn. Magn. Mater. **140**, 729 (1995).
[54] K. E. Johnson, R. J. Wilson, and S. Chiang, Phys. Rev. Lett. **71**, 1055 (1993).
[55] M. Getzlaff, M. Bode, R. Pascal, and R. Wiesendanger, Phys. Rev. B **59**, 8195 (1999).
[56] M. Bode, R. Pascal, M. Getzlaff, and R. Wiesendanger, Acta Phys. Pol. A **93**, 273 (1998).
[57] C. Busse, C. Polop, M. Müller, K. Albe, U. Linke, and T. Michely, Phys. Rev. Lett. **91**, 056103 (2003).
[58] A similar contrast due to stacking of Co on Cu(111) has been found by Pietzsch *et al.* (Ref. 8).
[59] P. Hohenberg and W. Kohn, Phys. Rev. **136**, 864 (1964).
[60] J. P. Perdew, K. Burke, and M. Ernzerhof, Phys. Rev. Lett. **77**,

3865 (1996).
[61] E. Wimmer, H. Krakauer, M. Weinert, and A. Freeman, Phys. Rev. B **24**, 864 (1981).
[62] http://www.flapw.de
[63] More precisely there are two bands being nearly degenerate. Nevertheless, they are due to only one surface band, but for each surface of the film, the upper and the lower. Due to the finite thickness of the film, there remains a small interaction, and the bands are only nearly degenerate.
[64] M. Pratzer and H. J. Elmers, Surf. Sci. **550**, 223 (2004).